nature materials

ARTICLES

PUBLISHED ONLINE: 23 MARCH 2015 | DOI: 10.1038/NMAT4247

Phonon-induced diamagnetic force and its effect on the lattice thermal conductivity

Hyungyu Jin[1], Oscar D. Restrepo[2], Nikolas Antolin[2], Stephen R. Boona[1], Wolfgang Windl[2], Roberto C. Myers[2,3,4] and Joseph P. Heremans[1,2,4]*

Phonons are displacements of atoms around their rest positions in a crystalline solid. They carry sound and heat, but are not classically associated with magnetism. Here, we show that phonons are, in fact, sensitive to magnetic fields, even in diamagnetic materials. We do so by demonstrating experimentally that acoustic phonons in a diamagnetic semiconductor (InSb) scatter more strongly from one another when a magnetic field is applied. We attribute this observation to the magnetic-field sensitivity of the anharmonicity of the interatomic bonds that govern the probability of phonon–phonon interactions. The displacements of atoms locally affect the orbital motion of valence band electrons, which, in the presence of an external magnetic field, spatially modulates the orbital diamagnetism around the displaced atoms. The spatial gradient in magnetic moment results in an anharmonic magnetic force exerted on the displaced atom. The process is modelled by *ab initio* calculations that, without the use of a single adjustable parameter, reproduce the observed 12% decrease in the lattice thermal conductivity under a 7 T magnetic field at a temperature of 5.2 K.

Electrons, phonons, and magnons (spin waves) are three elemental excitations in solids known to carry heat. Electrons are subject to a Lorentz force in the presence of an applied external magnetic field (H), giving rise to thermomagnetic effects[1]. The magnon density-of-states, heat capacity and thermal conductivity (κ) are affected by H (ref. 2). In ferromagnetic crystals lacking inversion symmetry, H can induce a Dzyaloshinskii–Moriya interaction that results in a magnon Hall effect[3]. It is only the phonon properties that are not conventionally considered to be sensitive to H, although some reports exist of thermomagnetic effects in insulating paramagnetic materials[4,5]. In contrast, we report here a magnetic response of the phonons in InSb, where the electronic states near the Fermi energy consist of only *s*- and *p*-electron shells, and attribute it to phonon-specific local diamagnetic moments on the atoms. These moments arise in the presence of an external magnetic field from phonon-induced changes in the valence band. Local and transient net moments then appear when phonon displacements are treated as effectively frozen in time (frozen-phonon approximation). They change continuously with time-dependent displacement, owing to the nearly instantaneous redistribution of electrons after changes in ionic-core position. Obviously, both the spatial and temporal averages of this phonon-induced diamagnetic moment are zero. Yet, as we show, the spatial gradient in this transient moment alters the interatomic forces and results in magnetic-field-sensitive bond anharmonicities and phonon–phonon interactions; mechanisms that have been at the root of the most recent progress in the design of thermoelectric materials[6–8].

Magnetic-field dependence of phonon–phonon interactions

We used large InSb single-crystal samples with heat flow (Q) and H aligned along the [100] direction. Below 10 K, their thermal conductivity is $\sim 200 \leq \kappa \leq \sim 2{,}700$ W m^{-1} K^{-1} and entirely due to phonons, with the electronic thermal conductivity being 10^5 times smaller than the phonon conductivity (see Supplementary Information). We mount each crystal in a tuning fork geometry[9,10] (Fig. 1a,b): measuring the phonon conductivity ratio between the arms of a tuning fork sample allows one to isolate different phonon scattering mechanisms from boundary effects. The tuning fork has a large arm and a small arm of cross-sectional areas A_L and A_S, through which heat fluxes Q_L and Q_S are sent, respectively. The tuning fork is the thermal equivalent of a galvanic potentiometer: when the ratio of the heat flows Q_L/Q_S is balanced so that $\Delta T_{DIFF} = 0$ (Fig. 1b), the ratio between the lattice thermal conductivities of the large and small arms (κ_L and κ_S, respectively) is $\kappa_L/\kappa_S = (Q_L/Q_S)/(A_L/A_S)$.

This measurement of κ_L/κ_S is independent of the calibration of the thermometers, of their H-dependence (see Supplementary Information), and of eventual heat losses, assuming that both arms have the same losses. Only the amount of heat delivered by the heaters needs to be measured accurately, allowing a resolution of 1 part in $\sim 10^4$ or better. Most importantly, we will show that κ_S is mostly due to ballistic phonon transport below 8 K in our samples, which provides a reference to isolate the physics of phonon–phonon interactions in the measured ratio κ_L/κ_S (ref. 10).

The ratio κ_L/κ_S is shown as a function of temperature in Fig. 1c at $H = 0$ and 7 T for the first sample (A). The error bars were calculated in detail by taking possible random, systematic and fitting errors into account (Supplementary Information). The observed change in κ_L/κ_S (12% at 7 T and 5.2 K) is well above the error bars. Figure 2a shows a repeat of the same measurement on sample B—the same sample after it had been cycled three times to room temperature and subjected to a considerable amount of thermal shock that induced dislocation strain fields in both arms that scatter phonons and strongly reduce κ. Both the ratio κ_L/κ_S and its H-dependence (6% below 4 K) are smaller than in sample A (Fig. 1c). The ratio κ_L/κ_S is shown as a function of H in Fig. 2b to be a monotonic and even function of H.

The thermal conductivity of the small arm of sample B, κ_S, is shown in Fig. 2c. The H-dependence of κ_L/κ_S is observed

[1]Department of Mechanical and Aerospace Engineering, The Ohio State University, Columbus, Ohio 43210, USA. [2]Department of Material Science and Engineering, The Ohio State University, Columbus, Ohio 43210, USA. [3]Department of Electrical and Computer Engineering, The Ohio State University, Columbus, Ohio 43210, USA. [4]Department of Physics, The Ohio State University, Columbus, Ohio 43210, USA. *e-mail: Heremans.1@osu.edu

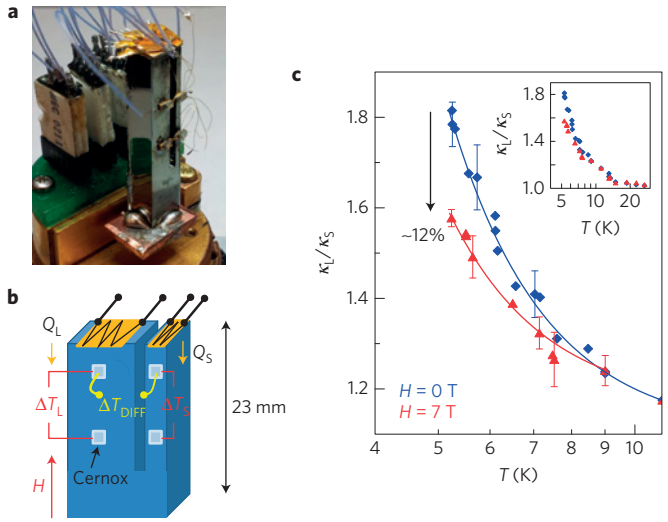

Figure 1 | Magnetic-field dependence of lattice thermal conductivity in InSb. a, InSb tuning fork with a large arm of cross-section A_L and a small arm of cross-section A_S. **b**, Principle of the tuning fork geometry: two heaters provide heat fluxes Q_L and Q_S. The measurements are made when the temperature difference between the arms is zero ($\Delta T_{DIFF}=0$)—that is, the condition $\kappa_L/\kappa_S=(Q_L/Q_S)/(A_L/A_S)$ holds. This gives an accurate measurement of the ratio κ_L/κ_S. **c**, Temperature dependence of κ_L/κ_S at zero magnetic field and in a longitudinal magnetic field of 7 T (sample A). The inset shows κ_L/κ_S over an extended temperature range. T denotes the average temperature of the sample, which, by the design of the tuning fork, is the same in the small and large arms. The error bars are standard deviations of the means, obtained as described in the Supplementary Information.

in the temperature range between 3 and 8 K, where $\kappa_S(T)$ is limited primarily by scattering on the boundaries of our particular samples and phonon conduction is essentially ballistic[11]. Deviations from ballistic phonon transport start to occur first in κ_L at these temperatures, and κ_S serves as an internal reference for all material properties of the sample except phonon–phonon interactions. From 3 to 8 K, phonons are scattered[11] by other phonons at a rate of τ_φ^{-1}, by dislocations at a rate of τ_D^{-1}, by point defects at a rate of τ_{PD}^{-1}, and by the sample's boundaries at a rate of τ_{BS}^{-1} in the small arm and τ_{BL}^{-1} in the large arm. Assuming that these scattering mechanisms operate independently of each other (Matthiessen's rule[11]), the total scattering rate is $\tau^{-1}=\tau_\varphi^{-1}+\tau_D^{-1}+\tau_{PD}^{-1}+\tau_B^{-1}$, where τ_B^{-1} is either τ_{BS}^{-1} or τ_{BL}^{-1} depending on which arm is considered. The kinetic formula[11] gives $\kappa=1/3Cv\ell=1/3Cv^2\tau$, where C is the specific heat, v the sound velocity, ℓ the mean free path ($\ell=v\tau$) and τ the scattering time. Rigorously, this formula has to be integrated over phonon modes and wavevectors q. In our geometry and temperature range, heat is carried principally by one longitudinal acoustic (LA) and two transverse acoustic (TA) modes with propagation velocities along [100] and essentially linear dispersion relations[12]. When these phonons interact with other phonons, τ_φ^{-1} involves phonons throughout the Brillouin zone (BZ; ref. 13). For this simple analysis, we consider the kinetic formula to be a mode and frequency average, and write

$$\frac{\kappa_L}{\kappa_S}=\frac{\frac{1}{3}Cv^2[\tau_\varphi^{-1}+\tau_D^{-1}+\tau_{PD}^{-1}+\tau_{BL}^{-1}]^{-1}}{\frac{1}{3}Cv^2[\tau_\varphi^{-1}+\tau_D^{-1}+\tau_{PD}^{-1}+\tau_{BS}^{-1}]^{-1}}$$

$$=\frac{\tau_\varphi^{-1}+\tau_D^{-1}+\tau_{PD}^{-1}+\tau_{BS}^{-1}}{\tau_\varphi^{-1}+\tau_D^{-1}+\tau_{PD}^{-1}+\tau_{BL}^{-1}} \quad (1)$$

Thus κ_L/κ_S is independent of C and v. We measure $C(T,H)$ (Fig. 2d) and observe that it is independent of H to within our experimental accuracy (2%). In the temperature range between 3 and 8 K, boundary scattering dominates in the small arm, but phonon–phonon scattering is more important in the large arm ($\tau_{BS}^{-1}>\tau_\varphi^{-1},\tau_{BL}^{-1}$; refs 9,10). Thus, equation (1) reduces to

$$\frac{\kappa_L}{\kappa_S}\approx\frac{\tau_D^{-1}+\tau_{PD}^{-1}+\tau_{BS}^{-1}}{\tau_\varphi^{-1}+\tau_D^{-1}+\tau_{PD}^{-1}+\tau_{BL}^{-1}} \quad (2)$$

τ_φ^{-1} and τ_D^{-1} are proportional[11] to the square of the Grüneisen parameter, which, for each mode i and frequency ω, is defined as $\gamma_i(\omega)\equiv \mathrm{d}\ln\omega/\mathrm{d}\ln V|_i$, the logarithmic derivative of the phonon angular frequency ω with respect to the volume V of the crystal. The thermal conductivity involves phonons and phonon interactions throughout the entire BZ. Therefore, τ_φ^{-1} and τ_D^{-1} depend on the mode- and frequency-averaged Grüneisen parameter γ weighted by the specific heat. γ quantifies the degree to which the bond forces deviate from simple harmonic behaviour and is temperature dependent: it changes sign in InSb below 5 K (refs 14,15). When two phonons collide in a solid with $\gamma\neq 0$, the presence of the first phonon locally modifies the acoustic properties for the second phonon, decreasing its transmission probability. The same reasoning applies to the interaction between a phonon and the strain field around a dislocation. As a result, it is given[11] that $\tau_\varphi^{-1},\tau_D^{-1}\propto\gamma^2$.

When dislocation scattering is less important than the other mechanisms (sample A), equation (2) shows that the effect of γ is limited to the denominator of κ_L/κ_S, even in the presence of point defect and boundary scattering in the large arm. In the ideal case of defect-free isotopically pure InSb with $A_L\to\infty$, $\tau_\varphi^{-1}\gg(\tau_{PD}^{-1},\tau_D^{-1},\tau_{BL}^{-1})$ and $\kappa_L/\kappa_S\approx\tau_{BS}^{-1}/\tau_\varphi^{-1}\propto\gamma^{-2}$, because τ_{BS}^{-1} is independent of temperature (as are the sample dimensions and the sound velocity). Dislocation scattering (sample B) and the presence of the other scattering mechanisms are expected to attenuate the effect of γ on κ_L/κ_S, as verified experimentally by comparing the effect on sample B (Fig. 2a) against that on sample A (Fig. 1c). In the following *ab initio* theory section, we neglect the effects of dislocations on sample A, and the resulting agreement between theory and experiment will justify this approach a posteriori. Note that the temperature dependence of the effect shown in Figs 1 and 2 arises from our choice of material and sample geometry. InSb was selected so that the observed effect would occur in a region where the tuning fork geometry is able to distinguish the anharmonic regime from the boundary scattering regime. The sample dimensions were then selected so as to isolate τ_φ^{-1} above 3 K. The fact that the effect is most pronounced between 3 and 8 K is not intrinsic but results from the selection of the experimental parameters, which is based on theoretical considerations given below.

We identify possible origins for the H-dependence of κ_L/κ_S as the electronic thermal conductivity or Peltier heat, phonon–electron interactions, an H-dependent phonon density-of-states, and an H-dependent phonon–phonon scattering rate via γ. Considering first the Peltier heat, the electronic contribution to the thermal conductivity is measured and calculated in the Supplementary Information. This effect is limited to $<6\times10^{-3}$ W m^{-1} K^{-1}, which is less than a 1:10^5 part of the total conduction. In the case of phonon–electron interactions, low-frequency phonons with wavevectors $k_{phonon}\sim k_{electron}$ can be scattered by electrons as the temperature decreases (the reciprocal effect of phonon-drag[16], which we observe; see Supplementary Information). If this effect were important, however, κ_L/κ_S would increase with H because the electrons in InSb freeze out in magnetic fields at low temperature (see Supplementary Information), which is the opposite of what we observe. We also rule out an H-dependent phonon density-of-states, as we observe no significant H-dependence to the specific heat (Fig. 2d). Indeed,

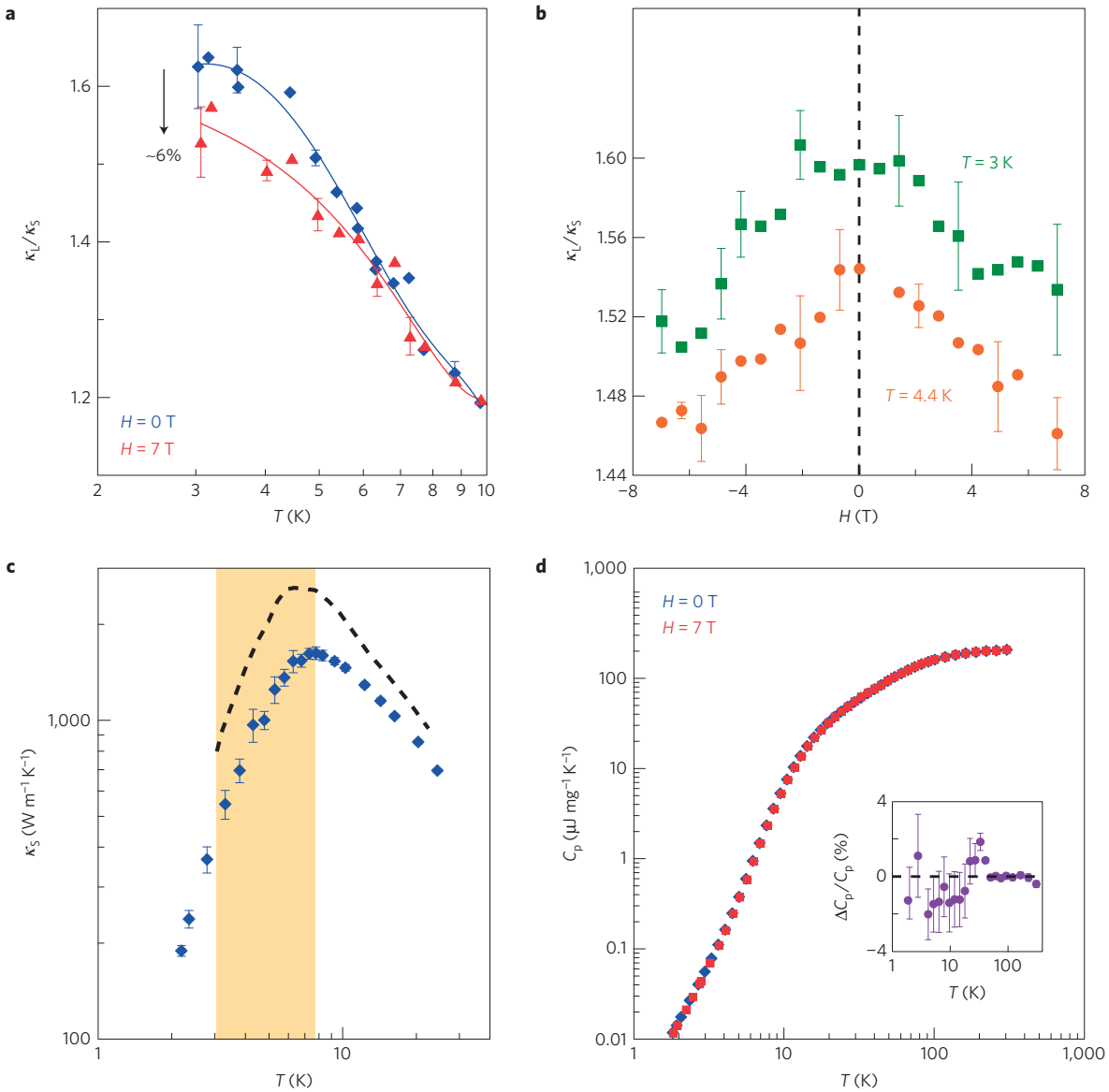

Figure 2 | Measurements on sample B with reduced thermal conductivity after thermal cycling. a, Temperature dependence of κ_L/κ_S at $H=0$ T and in a longitudinal field $H=7$ T. **b**, κ_L/κ_S is an even function of magnetic field, as expected from symmetry[25]. **c**, Temperature dependence of κ_S ($H=0$ T), measured using the heater-and-sink method. The dashed line shows κ_L calculated from κ_S and the ratio in **a**. The yellow shaded region indicates the temperature range where the effect of magnetic field on κ_L/κ_S is most pronounced. **d**, Temperature dependence of the specific heat of a piece of the same boule of InSb; the inset shows its relative change with field $\Delta C_p/C_p \equiv [C_p(7\,\mathrm{T}) - C_p(0\,\mathrm{T})]/C_p(0\,\mathrm{T})$, which is less than 2%, but not resolved above the noise level. The error bars are standard deviations of the means, obtained as described in the Supplementary Information. T denotes the average temperature of the sample.

at the temperatures of the experiment (<10 K) the LA and TA modes that contribute to the specific heat are also those that contribute to the thermal conductivity[12].

We therefore put forward the last hypothesis; that the H-dependence of γ gives rise to the H-dependence of κ_L/κ_S, such that

$$\frac{\Delta\left[\frac{\kappa_L}{\kappa_S}\right]}{\frac{\kappa_L}{\kappa_S}} \equiv \frac{\left(\frac{\kappa_L}{\kappa_S}\right)_{H=7\,\mathrm{T}} - \left(\frac{\kappa_L}{\kappa_S}\right)_{H=0\,\mathrm{T}}}{\left(\frac{\kappa_L}{\kappa_S}\right)_{H=0\,\mathrm{T}}} = -\frac{\Delta\left[\gamma^{-2}\right]}{\gamma^{-2}}$$

$$\equiv -\frac{\left(\gamma^{-2}\right)_{H=7\,\mathrm{T}} - \left(\gamma^{-2}\right)_{H=0\,\mathrm{T}}}{\left(\gamma^{-2}\right)_{H=0\,\mathrm{T}}} \qquad (3)$$

The phonon-induced diamagnetic anharmonic force

This hypothesis leads to a quantitative agreement between the experimental magnitude and temperature dependence of the effect and an *ab initio* calculation of a phonon-induced magnetic moment (Fig. 4). Because γ depends fundamentally on the interatomic potential (U), the H-dependence of γ must arise from an H-induced modification of U. Under the conditions where we observe H-dependent thermal properties, InSb contains negligible conduction electrons or valence band holes; it is insulating and without net spin. In such a solid, H can induce changes only in orbital angular momentum (L) of core electrons and the filled valence band. Such changes give rise to the Langevin diamagnetism, as well as virtual magnetic dipole transitions between energy levels in an LS multiple ($E(J) - E(J \pm 1)$), where S is the spin angular momentum and J the total angular momentum ($J = L + S$),

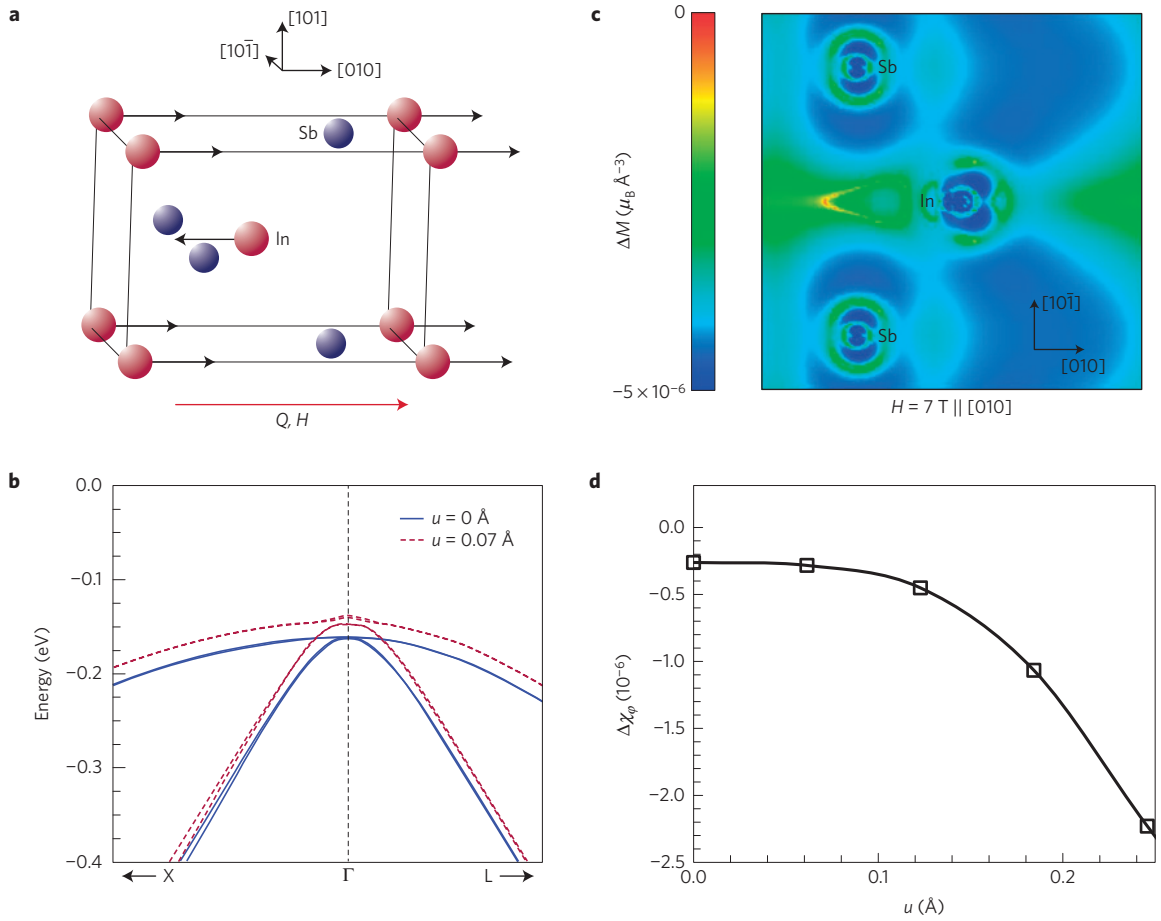

Figure 3 | *Ab initio* calculation of the magnetic moment of frozen phonons in InSb. a, The frozen-phonon picture, showing the atomic displacements of the In atoms for a longitudinal acoustic [010] mode. The red arrow indicates the direction of the heat flux (Q) and applied field (H). **b**, Calculated VB maximum in $H=20$ T (an unrealistically high value to visualize the effect), the blue lines with the atoms in their equilibrium positions, the red dotted lines with the atoms displaced by 0.07 Å as in **a**. **c**, Spatial distribution of the change in magnetic moment density (logarithmic mesh) in the plane normal to [101], calculated for an unrealistic 0.18 Å displacement of In atoms used to illustrate the effect. **d**, Calculated phonon-induced diamagnetic susceptibility $\Delta\chi_\varphi$, averaged over the unit cell as a function of atomic displacement u (the In atoms are displaced along [010]).

which is known as Van Vleck paramagnetism[17,18]. The magnetic susceptibility χ, which is the ratio of the induced magnetization (M) to H, is therefore given by

$$\chi = -\frac{\mu_0 NZe^2}{6m}\sum_{\text{core}}\langle r^2\rangle - \frac{\mu_0 NZe^2}{6m}\sum_{\text{valence}}\langle r^2\rangle + 2N\mu_0\mu_B^2\sum_{i\neq j}\frac{\left|\langle i|\,(L_z+g_0S_z)|j\rangle^2\right|}{E_i-E_j} \quad (4)$$

with μ_0 the magnetic permeability of free space, μ_B the Bohr magneton, N the density of atoms, Z the atomic number, m the free electron mass, r the atomic radius and g_0 the electronic g-factor. Considering the sensitivity of the three terms to phonon displacement, we can expect that the core susceptibility feels negligible influence. We expect the diamagnetic susceptibility, being driven by valence electron orbital motion, to be sensitive to the local bonding environment. Lande's interval rule indicates that transitions between $E(J)-E(J\pm1)$ are proportional to the magnitude of the spin–orbit coupling (SOC; ref. 18). Our calculations show that the change in SOC with atomic displacements is negligible (<1%), from which we conclude that the Van Vleck paramagnetic term does not couple to phonons. One then expects a local change $\Delta\chi_\varphi$ in χ due to the atomic displacements and bond distortions associated with a phonon. Accordingly, we label $\Delta\chi_\varphi$ the phonon-induced diamagnetic susceptibility. Under an applied field H, the diamagnetic response of the solid is altered locally around phonons; that is, phonons exhibit a diamagnetic moment $H\Delta\chi_\varphi$. However, phonon displacements are averaged to zero over time and space, which means the phonon moments must also sum to zero, although they can lead to magnetic-field sensitive local interactions with other phonons through these transient moments.

The quantitative picture we offer is based on the frozen-phonon model, whereby atomic motions occur at terahertz frequencies, which is a timescale much slower than that of electrons. The electrons therefore see the solid locally distorted by the phonon as a different crystal and develop a local perturbation of the band structure around the phonon. The conduction (CB) and valence bands (VB) are both affected. By considering equation (4) and the known sensitivity of χ to long-range Coulomb interactions, we postulate that the free electron mass in equation (4) can be replaced with the VB effective mass to approximate the effect of the VB structure on χ. By this mechanism, the band structure distortion associated with the phonon is proportional to $\Delta\chi_\varphi$ around the equilibrium position r_0 of an atom. This results in a local magnetic moment density $M(r)=H\chi(r)$ around that atom in an external applied magnetic field, and a magnetic force $F_M(r)=\nabla[M(r)\cdot H]=H^2\nabla\chi(r)$ that adds to the interatomic force F_0. If we assume that F_0 is harmonic and characterized by a

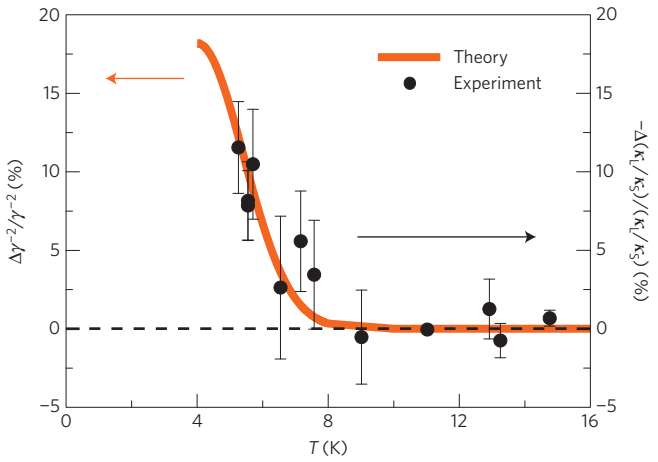

Figure 4 | Agreement between *ab initio* theory and experiment. Temperature dependence of the *ab initio* calculated relative change in Grüneisen parameter with field ($\Delta[\gamma^{-2}]/\gamma^{-2}$) is compared against the experimentally observed change in ratio κ_L/κ_S, using equation (3). The field is changed from 0 to 7 T. The $\gamma(T)$ values are from ref. 14. The agreement, which involves no adjustable parameters, is evidence for the existence of phonon-induced diamagnetism and its role in phonon–phonon interactions. The error bars are standard deviations from the means.

spring constant K ($F_0 = Kr$) independent of r, then the total force $F = Kr + F_M(r)$ is no longer harmonic, and an H-dependent contribution to γ of the order $\Delta\gamma(H) \propto H^2\nabla\nabla\chi(r)$ is expected.

The above model is tested using *ab initio* density functional theory (DFT) modelling in an applied magnetic field H carried out in three steps considering the LA and two TA phonon modes described above. First, the average atomic displacements are calculated using *ab initio* molecular dynamics, and are found to be of the order[19] of 0.05 Å in the low-temperature limit ($T < 30$ K, numerical values given in the Supplementary Information). Second, band structure calculations in H with the ELK (refs 20,21) code (see Methods) for displaced frozen-phonon cells reveal changes in CB and VB. In the presence of the frozen phonon shown in Fig. 3a with In atoms displaced by 0.07 Å, Fig. 3b shows that the VB effective mass decreases by 5% in $H = 20$ T. Finally, the magnetic moment $M(r)$, integrated over the unit cell, is calculated to be $M = -50m\mu_B$ for $H = 20$ T when the atoms are in their equilibrium positions. This corresponds well to the diamagnetic susceptibility ($\chi = -2.46 \times 10^{-7}$) of InSb. With the displacement of 0.07 Å, the value of M increases by 8% to $M = -54m\mu_B$. Figure 3c shows that the local variation of $M(r)$ in the ([010], [10$\bar{1}$]) plane due to the atomic motion of Fig. 3a is very localized around the In and Sb atoms: this creates a strong spatial gradient of $M(r)$. The vector potential $\mathbf{A}$ in the Hamiltonian of the interaction (see Supplementary Information) is identified as the physical origin of the phonon-induced local diamagnetic moment. This can be specifically written as $\Delta\chi_\varphi = -(Ne^2/4mc^2H^2)\mathbf{A}^2(r_i)$. Figure 3d shows $\Delta\chi_\varphi$ as a function of atomic displacement. At small, experimentally accessible displacements of $u < 0.1$ Å, both CB and VB move, but the gap does not close. The change $\Delta\chi_\varphi$ is mainly phonon-induced Langevin diamagnetism (equation (4); ref. 17). At very high displacements ($u > 0.18$ Å, presently beyond the reach of experiments), the frozen phonon can move the CB and VB so as to close the energy gap. Free electrons and holes appear, resulting in additional Landau diamagnetism. This observation relates the effect we describe here to the magnetostriction observed at high field in diamagnetic solids[22,23] to track the de Haas–van Alphen effect. At the lower fields where the present experiments are carried out, the field only insignificantly affects the bond lengths or the phonon frequencies themselves, yet its effect on the derivative of the phonon frequencies is still important. Effects of electronic properties that are insignificant on the phonon frequencies themselves but strongly affect the Grüneisen parameters have been observed in both semiconductors[8] and metals[24].

Applying the procedure outlined above to the *ab initio* values of $M(r)$, we derive H-dependent values of γ integrated over the unit cell, and directly compare experiment and theory. Figure 4 shows the ratio $\Delta[\gamma^{-2}]/\gamma^{-2}$ calculated *ab initio* using $\gamma(T)$ from ref. 14 with no adjustable parameters. This is compared (equation (3)) to the experimental H-dependence of κ_L/κ_S. We submit that the agreement supports the hypothesis. Note that the phonon-induced diamagnetic moment itself is, to the first order, independent of temperature. Indeed, the movement of the atoms around their equilibrium positions below 10 K in InSb is due to a temperature-independent quantum effect—the zero-point vibrations[19]—and diamagnetism arises from the valence band, which has no temperature-dependence other than through atomic motion[19]. The relative effect of the phonon-induced diamagnetic moment on γ is most pronounced at temperatures where the background γ is small and the thermal expansion coefficient crosses zero—that is, ~4 K in InSb (ref. 14). This determines the overall temperature dependence of the experimentally observed effect.

Outlook

We identify a magnetic-field response of the lattice thermal conductivity experimentally, and attribute it to a specific phonon-induced diamagnetic moment. This local diamagnetism is small and does not result in a net magnetic moment, because both spatial and temporal averages of this moment are zero. However, its very sharp spatial gradient results in an anharmonic force applied to the atoms in the solid that is intense enough to be measured in the thermal properties. It is likely that this phonon-induced diamagnetism is a universal property of all solids, and it is plausible that it may be a yet undiscovered mechanism for coupling between phonons, heat and magnetic systems.

Methods

The starting material for the samples is an InSb boule doped with Te to an electron concentration of 1.3×10^{15} cm^{-3} (measured by Hall effect at temperatures $3\,K < T < 50$ K). Magnetization measurements on a piece of the same boule showed that no magnetic impurities are present in the samples down to our sensitivity limit of 16 ppb. The electronic transport and magnetic properties of the material are given in the Supplementary Information. The samples are cut into the tuning fork geometry shown in Fig. 1. The large arm has a cross-section $A_L \sim 4 \times 3$ mm^2, and the small arm has $A_S \sim 4 \times 1$ mm.^{2} The length of both arms is 17.3 mm. The sample was mounted on a heat sink, with the small arm equipped with one 120 Ω heater and the large arm with three heaters. Each arm was equipped with $0.965 \times 0.762 \times 0.203$ mm^3 Cernox thermometers, as shown, which were calibrated as a function of temperature (their field dependence was also previously characterized). We fixed the power Q_L on the large arm and adjusted the heater power on the small arm (Q_S) until $\Delta T_{DIFF} = 0$ (see Fig. 1b). At this value of Q_S, the thermal conductivity ratio $\kappa_L/\kappa_S = (Q_L/Q_S)/(A_L/A_S)$, where κ_L and κ_S denote the thermal conductivities, and A_L and A_S the cross-sectional areas of the large and small arms, respectively. The area ratio (A_L/A_S) is determined accurately from the high-temperature asymptote of Q_L/Q_S. A detailed description of this method and an analysis of the errors it accrues, which determines the error bars in Figs 1 and 2, is provided in the Supplementary Information with a detailed description of how the magnetic-field dependence of the Cernox thermometers is eliminated from the measurements. The lowest temperature of all experiments is limited by the cooling power of the cryostat and the fact that the thermal resistance between the sample and the cryostat is much larger than that of the sample itself. Consequently, the heat flux necessary to create a gradient across the sample also increases the sample's average temperature considerably above that of the cryostat. As a result, for example, the lowest temperature that could be reached on the sample B with dislocations (Fig. 2a) is lower than that of the more pristine sample A (Fig. 1c).

The thermal conductivity in Fig. 2c was measured using the classical heater-and-sink method on the small arm of sample B, which is the sample that had the lowest κ in the experiment, for the same reason: all other arms either require large heater powers or give small gradients. The thermal conductivity of

the large arm (κ_L) of sample B was then calculated from κ_S and the ratio in Fig. 2a; more details are given in the Supplementary Information.

No transverse thermal gradient due to the phonon Hall effect[4] is expected to perturb the measurement, because in our configuration the magnetic field is parallel to the flux. In that configuration the transverse gradient was shown experimentally[4] to be zero, as expected theoretically from the Onsager relations[25].

The ELK program is an all-electron, full-potential, linearized augmented-plane wave code[20,21]. It allows inclusion of non-collinear magnetism with arbitrary external magnetic fields. We checked the convergence of our results by performing calculations with an increasing number of k-points in the BZ. We found that including 20 empty states in our calculations gives us an accuracy of better than 1%. To verify accuracy we used $31 \times 31 \times 23$ k-point meshes. Our results show that the change in magnetic moment is less than 20% from $15 \times 15 \times 11$ k-point meshes. We used the latter in our calculations as they represent a significant decrease in the computational demands and do not change our overall conclusions. We verify that the local magnetic moment $M(r)$ is linear in applied field (see Supplementary Fig. 11), so that the susceptibility $\chi(r)$ is independent of field and the moment is given by $M(r) = H\chi(r)$. The calculated value of γ is the mode and frequency average over the whole BZ, weighted by the specific heat (see Supplementary Information). We used the experimental value of Hass *et al.*[26] for the phonon linewidth and expressed it as an energy smearing equivalent to a temperature of 2 K (see Supplementary Information); this value affects the lineshape, but not the magnitude, of the calculated line in Fig. 4. We point out that the agreement in Fig. 4 would have had an offset along the x-axis of 2 K had we used the $\gamma(T)$ data of ref. 15, as also described in the Supplementary Information. Supplementary Movie 1 illustrates the local magnetic moments in the plane normal to the [101] axis around In and Sb atoms moving during the passage of a LA [010] phonon.

Received 14 October 2014; accepted 2 February 2015; published online 23 March 2015

References

1. Harman, T. C. & Honig, J. M. *Thermoelectric and Thermomagnetic Effects and Applications* (McGraw-Hill, 1967).
2. Boona, S. R., Myers, T. C. & Heremans, J. P. Spin caloritronics. *Energy Environ. Sci.* **7,** 885–910 (2014).
3. Onose, Y. *et al.* Observation of the magnon Hall effect. *Science* **329,** 297–299 (2010).
4. Strohm, C., Rikken, G. L. J. A. & Wyder, P. Phenomenological evidence for the phonon Hall effect. *Phys. Rev. Lett.* **95,** 155901 (2005).
5. Morton, I. P. & Rosenberg, H. M. Scattering of phonons by spins at low temperatures. *Phys. Rev. Lett.* **8,** 200–201 (1962).
6. Zhao, L-D. *et al.* Ultralow thermal conductivity and high thermoelectric figure of merit in SnSe crystals. *Nature* **508,** 373–377 (2014).
7. Heremans, J. P. The ugly duckling. *Nature* **508,** 327–328 (2014).
8. Nielsen, M. D., Ozolins, V. & Heremans, J. P. Lone pair electrons minimize lattice thermal conductivity. *Energy Environ. Sci.* **6,** 570–578 (2013).
9. Geballe, T. H. & Hull, G. W. in *Conference de physique des basses temperatures, Institut international du froid, Paris* 460–463 (1955).
10. Issi, J-P., Michenaud, J-P. & Heremans, J. P. in *Thermal Conductivity 14* (eds Klemens, P. G. & Chu, T. K.) 127–133 (Conference Proceedings, Plenum Press, 1976).
11. Berman, R. *Thermal Conduction in Solids* (Clarendon Press, 1976).
12. Price, D. L., Rowe, J. M. & Nicklow, R. M. Lattice dynamics of grey tin and indium antimonide. *Phys. Rev. B* **3,** 1268–1279 (1971).
13. Broido, D. A., Ward, A. & Mingo, N. Lattice thermal conductivity of silicon from empirical interatomic potentials. *Phys. Rev. B* **72,** 014308 (2005).
14. Sparks, P. W. & Swenson, C. A. Thermal expansions from 2 to 40 K of Ge, Si, and four III–V compounds. *Phys. Rev.* **163,** 779–790 (1967).
15. Cetas, T. C., Tilford, C. R. & Swenson, C. A. Specific heats of Cu, GaAs, GaSb, InAs, and InSb from 1 to 30 K. *Phys. Rev.* **174,** 835–844 (1968).
16. Puri, S. M. & Geballe, T. H. Phonon drag in n-type InSb. *Phys. Rev.* **136,** A1767–A1774 (1964).
17. Hudgen, S., Kastner, M. & Fritzsche, H. Diamagnetic susceptibility of tetrahedral semiconductors. *Phys. Rev. Lett.* **33,** 1552–1555 (1974).
18. Nolting, W. & Ramakanth, A. *Quantum Theory of Magnetism* (Springer, 2009).
19. Olguín, D., Cardona, M. & Cantarero, A. Electron–phonon effects on the direct band gap in semiconductors: LCAO calculations. *Solid State Commun.* **122,** 575–589 (2002).
20. Dewhurst, J. K. *et al.* Elk FP-LAPW code, version 2.2.9 (2004); http://elk.sourceforge.net
21. Sharma, S. *et al.* Comparison of exact-exchange calculations for solids in current-spin-density- and spin-density-functional theory. *Phys. Rev. B* **76,** 100401 (2007).
22. Heremans, J., Michenaud, J-P., Shayegan, M. & Dresselhaus, G. Magnetostriction and deformation potentials in graphite. *J. Phys. C* **14,** 3541–3546 (1981).
23. Michenaud, J-P., Heremans, J., Shayegan, M. & Haumont, C. Magnetostriction of bismuth in quantizing magnetic fields. *Phys. Rev. B* **26,** 2552–2559 (1982).
24. Souvatzis, P., Eriksson, O. & Katsnelson, M. I. Anomalous thermal expansion in α-titanium. *Phys. Rev. Lett.* **99,** 015901 (2007).
25. Akgöz, Y. C. & Saunders, G. A Space-time symmetry restrictions on the form of transport tensors: I. Galvanomagnetic effects. *J. Phys. C* **8,** 1387–1396 (1975).
26. Hass, M. & Henvis, B. W. Infrared lattice reflection spectra of III–V compound semiconductors. *J. Phys. Chem. Solids* **23,** 1099–1104 (1962).

Acknowledgements

The experiments were supported as part of the ARO MURI under award number W911NF-14-1-0016, US AFOSR MURI under award number FA9550-10-1-0533 (H.J.) and the NSF grant CBET-1133589 (J.P.H., R.C.M.). The theoretical work was supported by the NSF MRSEC program under grant DMR 1420451, as well as an allocation of computing time from the Ohio Supercomputing Center. We acknowledge help from Z. Yang and useful discussions with S. Barnes.

Author contributions

The experiments were designed and carried out by H.J. and J.P.H., the theory by J.P.H., W.W., R.C.M., S.R.B., N.A. and O.D.R., and all DFT computations by N.A., O.D.R. and W.W. All contributed to the integration between theory and experiment, and in writing the manuscript.

Additional information

Supplementary information is available in the online version of the paper. Reprints and permissions information is available online at www.nature.com/reprints. Correspondence and requests for materials should be addressed to J.P.H.

Competing financial interests

The authors declare no competing financial interests.